Formation of Nitrogen-Containing Polycyclic Cations by Gas-Phase and Intracluster Reactions of Acetylene with the Pyridinium and Pyrimidinium Ions

ARTICLE *in* JOURNAL OF THE AMERICAN CHEMICAL SOCIETY · DECEMBER 2012

Impact Factor: 12.11 · DOI: 10.1021/ja3068116 · Source: PubMed

5 AUTHORS, INCLUDING:

Abdel Rahman Soliman
Virginia Commonwealth University
13 PUBLICATIONS **61** CITATIONS
SEE PROFILE

Ahmed Hamid
Pacific Northwest National Laboratory
24 PUBLICATIONS **93** CITATIONS
SEE PROFILE

Isaac Attah
Virginia Commonwealth University
14 PUBLICATIONS **25** CITATIONS
SEE PROFILE

M. Samy El-Shall
Virginia Commonwealth University
272 PUBLICATIONS **4,604** CITATIONS
SEE PROFILE

JACS
JOURNAL OF THE AMERICAN CHEMICAL SOCIETY
Article
pubs.acs.org/JACS

Formation of Nitrogen-Containing Polycyclic Cations by Gas-Phase and Intracluster Reactions of Acetylene with the Pyridinium and Pyrimidinium Ions

Abdel-Rahman Soliman,[†] Ahmed M. Hamid,[†] Isaac Attah,[†] Paul Momoh,[†] and M. Samy El-Shall*[,†,‡]

[†]Department of Chemistry, Virginia Commonwealth University, Richmond, Virginia 23284-2006, United States
[‡]Department of Chemistry, Faculty of Science, King Abdulaziz University, Jeddah 21589, Saudi Arabia

Supporting Information

ABSTRACT: Here, we present evidence from laboratory experiments for the formation of nitrogen-containing complex organic ions by sequential reactions of acetylene with the pyridinium and pyrimidinium ions in the gas phase and within ionized pyridine−acetylene binary clusters. Additions of five and two acetylene molecules onto the pyridinium and pyrimidinium ions, respectively, at room temperature are observed. Second-order rate coefficients of the overall reaction of acetylene with the pyridinium and pyrimidinium ions are measured as 9.0×10^{-11} and 1.4×10^{-9} cm^3 s^{-1}, respectively, indicating reaction efficiencies of about 6% and 100%, respectively, at room temperature. At high temperatures, only two acetylene molecules are added to the pyridinium and pyrimidinium ions, suggesting covalent bond formation. A combination of ion dissociation and ion mobility experiments with DFT calculations reveals that the addition of acetylene into the pyridinium ion occurs through the N-atom of the pyridinium ion. The relatively high reaction efficiency is consistent with the absence of a barrier in the exothermic N−C bond forming reaction leading to the formation of the $C_7H_7N^{\bullet+}$ covalent adduct. An exothermic addition/H-elimination reaction of acetylene with the $C_7H_7N^{\bullet+}$ adduct is observed leading to the formation of a bicyclic quinolizinium cation ($C_9H_8N^+$). Similar chemistry is observed in the sequential reactions of acetylene with the pyrimidinium ion. The second acetylene addition onto the pyrimidinium ion involves an exclusive addition/H-elimination reaction at room temperature leading to the formation of a bicyclic pyrimidinium cation ($C_8H_7N_2^+$). The high reactivity of the pyridinium and pyrimidinium ions toward acetylene is in sharp contrast to the very low reactivity of the benzene cation, which has a reaction efficiency of 10^{-4}−10^{-5}. This indicates that the presence of a nitrogen atom within the aromatic ring enhances the ring growth mechanism by the sequential addition of acetylene to form nitrogen-containing polycyclic hydrocarbon ions. The observed reactions could explain the possible formation of nitrogen-containing complex organics by gas-phase ion−molecule reactions involving the pyridinium and pyrimidinium ions with acetylene under a wide range of temperatures and pressures in astrochemical environments such as the nitrogen-rich Titan's atmosphere. The current results suggest searching for spectroscopic evidence for these organics in Titan's atmosphere.

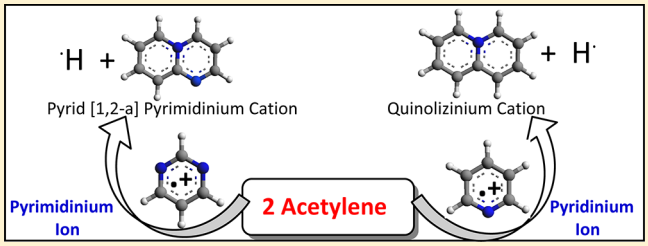

INTRODUCTION

Organic chemistry plays important roles in flames and combustion processes particularly for the mechanisms of soot formation and the generation of organic aerosol throughout the atmosphere, as well as in interstellar clouds and in the solar nebula particularly for the origin of the observed complex organics. Astronomical observations show that interstellar clouds and solar nebulae contain diverse organics, including methane, acetylene, benzene, polycyclic aromatic hydrocarbons (PAHs), and polycyclic nitrogen-containing aromatic hydrocarbons (PNAHs).[1−14] Gas-phase radical chemistry, ion−molecule and intracluster reactions, and catalysis on dust particles are important synthetic pathways for the formation of complex molecules in space environments.[4−8,11−26] Because molecules in outer space are subject to ionizing radiation, and reaction rates of ion−molecule reactions exceed by orders of magnitude those of gas-phase neutral reactions at the low interstellar temperature near 10 K, ion chemistry becomes increasingly competitive to gas-phase neutral chemistry in cold ionizing environments.[27−32] Unlike interstellar clouds, higher gas densities in the nebula can allow three-body processes that form adducts and clusters. These processes can lead to complex organics, clustering, and polymerization that produce nucleation centers for the formation of grains.[16,18,24,25,33−35] Similar organic chemistry occurs in Titan's atmosphere where a series of chemical reactions and physical processes could lead to the formation of complex organics starting from methane and nitrogen under the influence of solar UV radiation and energetic particles.[4,16,28,33−35] For example, the discovery of benzene on Titan[4,36] has raised the possibility of the formation of PAH cations and other complex organics made of hundreds of carbon atoms that could be responsible

Received: July 12, 2012
Published: December 3, 2012

   dx.doi.org/10.1021/ja3068116 | J. Am. Chem. Soc. 2013, 135, 155−166

for the unidentified infrared bands (UIBs)[19,37,38] and the diffuse interstellar bands.[39] In addition to benzene, large mass positive and negative ions were discovered on Titan,[4,40−44] which were attributed to fused-ring polycyclic aromatic hydrocarbon compounds such as naphthalene and anthracene and suggested that these are the precursors to the haze particles that form the optically thick haze layer lower in Titan's atmosphere.[4,40−44]

The wide range of temperature and pressure conditions in solar nebula allows diverse and unique chemistry to take place.[17,45,46] Fast ion−molecule reactions without barriers are possible in the low-temperature, low-density outer nebula. Other reactions with energy barriers can be allowed in the warmer zones of the nebula.[47,48] For example, we recently discovered new sequential reactions of acetylene with the benzene radical cation at higher temperatures (600 K) leading to the formation of naphthalene-type ions.[49] Interestingly, no reaction leading to covalent addition is observed at room temperature, and even the associated $C_6D_6^{\bullet+}(C_2H_2)$ products are not observed due to weak binding.[50] The barrier to the covalent addition of acetylene onto the benzene radical cation ($C_6H_6^{\bullet+}$) originates from the presence of six C−H bonds in the benzene cation and the absence of an available addition site.[51−53] Ring growth can also occur by the reactions of ionized heterocyclics with unsaturated hydrocarbons.[51−54] For example, we recently reported new cross reactions between the benzene radical cation and pyridine or pyridine radical cation and benzene resulting in efficient formation of a covalent bonded benzene−pyridine radical cation with a stable N−C bond.[55] These reactions may represent a general class of addition reactions that can form complex PNAHs in ionizing environments and in space. Simulations of a nitrogen rich atmosphere, such as that of Titan's, suggest that the nitrogen will be incorporated easily in the aromatic ring and predict that this process is barrierless and exothermic.[52] DFT calculations indicate that substitution of a carbon atom with nitrogen in the benzene cation ring leads to lowering or eliminating the barrier to the acetylene addition.[51−53] Therefore, one may expect the reaction of acetylene with the pyridinium ion ($C_5NH_5^{\bullet+}$) to be much faster than the reaction with the benzene radical cation. However, these theoretical predictions have not been confirmed by experimental observation because there is no report in the literature on the sequential reactions of acetylene with the pyridinium ion at different temperatures in the high pressure regime. Surprisingly, very little experimental work, in general, has been reported on the sequential reactions of acetylene with ionized aromatics at different temperatures and pressures.

As part of our program to study the reactions of acetylene with ionized aromatics that could lead to the formation of PAH and PNAH cations, we investigated the reactions of the acetylene with the pyridinium and pyrimidinium ions under gas-phase thermal conditions and within ionized pyridine−acetylene binary clusters using the mass-selected ion mobility technique.[49,55−58] Here, we report experimental evidence for the efficient formation of nitrogen-containing cyclic organics by the sequential addition of acetylene onto the $C_5NH_5^{\bullet+}$ and $C_4N_2H_4^{\bullet+}$ ions. The observed reactions could contribute to the formation of complex organics such as PAHs and PNAHs found in a wide variety of locations ranging from flames and combustion processes to interstellar space.[2,4,7,25,17,21,42]

EXPERIMENTAL SECTION

The experiments were performed using the VCU mass-selected ion mobility tandem mass spectrometer (Figure S1, Supporting Information). The details of the instrument can be found in several publications,[55−60] and only a brief description of the experimental procedure is given here. The molecular ions (pyridinium $C_5H_5N^{\bullet+}$ (m/z 79), deuterated pyridinium $C_5D_5N^{\bullet+}$ (m/z 84), or pyrimidinum $C_4H_4N_2^{\bullet+}$ (m/z 80)) were generated by 50 eV electron impact ionization (EI) following the supersonic beam expansion of the corresponding vapor mixture of 0.2% pyridine, d-pyridine, or pyrimidine in 4−5 bar of ultra pure helium through a 500 μm diameter pulsed nozzle (General Valve, Series 9), in pulses of 150−300 μs duration at repetition rates of 50−100 Hz, into a source chamber (10^{-8} mbar). The ions of interest were mass-selected by a quadrupole mass filter, and the beam was chopped into small pulses (5−15 μs pulses) and injected into the drift cell (5 cm long) containing a purified acetylene−helium mixture or pure purified acetylene gas at known pressures and temperatures. For the pyridine−acetylene binary clusters experiments, helium seeded with <3% purified acetylene gas was flowed through a glass bubbler containing pyridine or d-pyridine cooled to 200 K before expansion into the source chamber. The molecular or cluster ions of interest were mass-selected and injected into the drift cell containing ultra pure helium for mobility measurements. Flow controllers (MKS no. 1479A) were used to maintain a constant pressure inside the drift cell within ±1 mTorr. The temperature of the drift cell can be controlled to better than ±1K using four temperature controllers.

The injection energies used in the experiments (10−14 eV, laboratory frame) are slightly above the minimum energies required to introduce the ions into the cell against the He or C_2H_2/He outflow from the entrance orifice. Most of the ion thermalization occurs outside the cell entrance by collisions with He atoms or C_2H_2 molecules escaping from the cell entrance orifice. At a cell pressure of 0.2 Torr, the number of collisions that the $C_5H_5N^{\bullet+}$ encounters with the neutral molecules within 1−2 ms residence time inside the cell is more than 10^4 collisions, which is sufficient to ensure efficient thermalization of the $C_5H_5N^{\bullet+}$ ions. Further evidence for ion thermalization is obtained by observing the time-dependent product distribution as a function of injection energy.

Arrival time distributions (ATDs) of the various ions are measured by monitoring the signal corresponding to each ion as a function of time after injection into the cell. Pseudo first-order rate constants k_1 are calculated using the following relation $\ln I/(\sum I) = -kt$, where I is the integrated intensity of the reactant ATD peak, $\sum I$ is the sum of the intensities of the ATDs of reactant and all product ions including the secondary products, and t is the mean drift time taken as the center of the ATD of the reactant ion. k_1 is obtained from the slope of $-\ln I/(\sum I)$ versus t, where the reaction time is varied by varying the drift cell voltage. Second-order rate constant k_2 is obtained from $k_2 = k_1/[N]$, where N is the number density (molecules cm^{-3}) of the neutral reactant (C_2H_2) calculated from the measured partial pressure of the reactant inside the drift cell at a given temperature. All of the rate coefficients were replicated several times, and the estimated errors are calculated on the basis of the uncertainties in the measurements of the neutral reactant pressure and temperature in addition to fluctuations in ion signal and background noise.

The mobility K of an ion is defined as $K = \vec{v}_d/\vec{E}$, where $\vec{v}_d$ is the drift velocity and $\vec{E}$ is the field across the drift region.[60,61] Ion mobility measurements are carried out by injecting an ion pulse (10−50 μs) into the drift cell. ATDs are collected at different P/V values, where P is the pressure of the He buffer gas in the drift cell in Torr and V is the drift voltage in volts, by varying V while keeping P fixed. The plot of the mean arrival time (assuming Gaussian peak shape) versus P/V gives a straight line, and the reduced mobility is calculated from the slope of the line using the relation:[57,60,61]

$$t = \frac{z^2 \times 273.15}{T \times 760 \times K_o}\frac{P}{V} + t_0 \quad (1)$$

dx.doi.org/10.1021/ja3068116 | J. Am. Chem. Soc. 2013, 135, 155−166

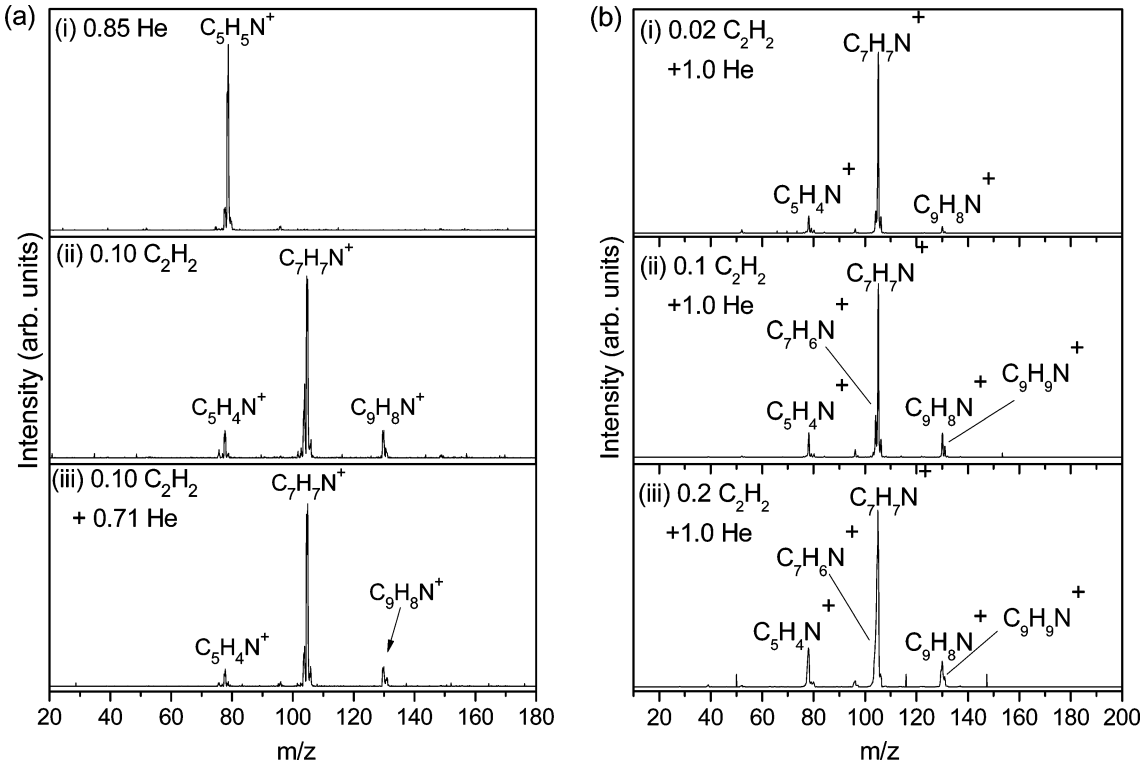

Figure 1. (a) Mass spectra obtained upon the injection of the mass-selected pyridinium ion ($C_5H_5N^{\bullet+}$) into the drift cell containing different partial pressures of helium and purified acetylene (in Torr) as indicated at 302 K. The injection energy used was 10.6 eV (lab frame), and the field across the cell was 5 V cm^{-1}. (b) Mass spectra obtained upon the injection of the mass-selected pyridinium ion ($C_5H_5N^{\bullet+}$) into the drift cell containing 1 Torr of helium and different amount of purified acetylene (in Torr) as indicated at 303 K. The injection energy used was 26.0 eV (lab frame), and the field across the cell was 4.0 V cm^{-1}.

where t is the mean arrival time, z is the drift cell length, T is the cell temperature in Kelvin, K_o is the reduced mobility (scaled to the number density at standard temperature and pressure STP), and t_o is the time that the ions spend outside the drift cell. All the mobility measurements are carried out in the low-field limit where the ion's drift velocity is small as compared to the thermal velocity and the ion mobility is independent of the field strength ($E/N < 6.0$, where E is the electric field intensity and N is the gas number density and E/N is expressed in units of Townsend (Td) where 1 Td = 10^{-17} V cm^2).[61] The average collision cross section, $\Omega^{(1,1)}$, of the ions in the helium buffer gas is calculated according to the kinetic theory:

$$K = \frac{3qe}{16N}\left(\frac{2\pi}{k_B T_{eff}}\right)^{1/2}\left(\frac{M_i + M_b}{M_i M_b}\right)^{1/2}\frac{1}{\Omega^{(1,1)}_{avg}} \quad (2)$$

where qe is the ion charge, N is the number density of the buffer gas, T_{eff} is the effective temperature, M_i and M_b are the masses of the ion and buffer gas, respectively, and $\Omega^{(1,1)}_{avg}$ is the orientationally averaged collision integral.

THEORETICAL SECTION

DFT calculations at the UB3LYP/6-31G* level were used to determine the structures and relative energies of several $C_7H_7N^{\bullet+}$ and $C_9H_9N^{\bullet+}$ adducts using the Gaussian 03 program.[62] The optimized structures were confirmed to be minima by vibrational frequency analysis. Theoretical calculations of possible structural candidates of the mass-selected ions are used to compute angle-averaged Ω's at different temperatures (for comparison with the measured values) using the trajectory method, which employs Lennard-Jones potential and ion-induced dipole interactions as described in the MOBCAL program.[63]

RESULTS AND DISCUSSION

1. Gas-Phase Reactions of Acetylene with the Pyridinium Ion. Figures 1a and b display the mass spectra obtained following the injection of the pyridinium ion $C_5H_5N^{\bullet+}$ into the drift cell containing helium carrier gas in the absence and presence of acetylene using low and high injection energies. As shown in Figure 1a(i), in the presence of pure helium, only the molecular pyridine ion is observed with no fragmentation, confirming the absence of excess ionization and injection energies, which could lead to the fragmentation of the ion. EI ionization of pyridine under the high pressure conditions of the supersonic beam expansion of the pyridine/helium mixture leads to the deposition of a small amount of energy on the ions as evident by the absence of any fragments upon the injection of the ions into the drift cell. Upon the injection of the pyridinium ions using the minimum injection energy (10.6 eV, lab frame) into pure acetylene (0.1 Torr), the C_2H_2 molecules react rapidly with the pyridinium ions to generate the first adduct $C_7H_7N^{\bullet+}$ (m/z 105) and dehydrogenated second adduct $C_9H_8N^+$ (m/z 130), in addition to a small amount of the dehydrogenated pyridine ion $C_5H_4N^+$ (m/z 78) as shown in the mass spectra displayed in Figure 1-a(ii). The same product ions are also observed in the presence of 0.71 Torr helium as shown in Figure 1a(iii). Similar ions are also observed in the presence of 1.0 Torr helium and variable amounts of acetylene even when higher injection energy (26 eV, lab frame) is used as shown in Figure 1b. This indicates that in the presence of sufficient third body buffer gas, the injected pyridine and the pyridine−acetylene adduct ions can be thermalized by collisional stabilization, and therefore the product

dx.doi.org/10.1021/ja3068116 | J. Am. Chem. Soc. 2013, 135, 155−166

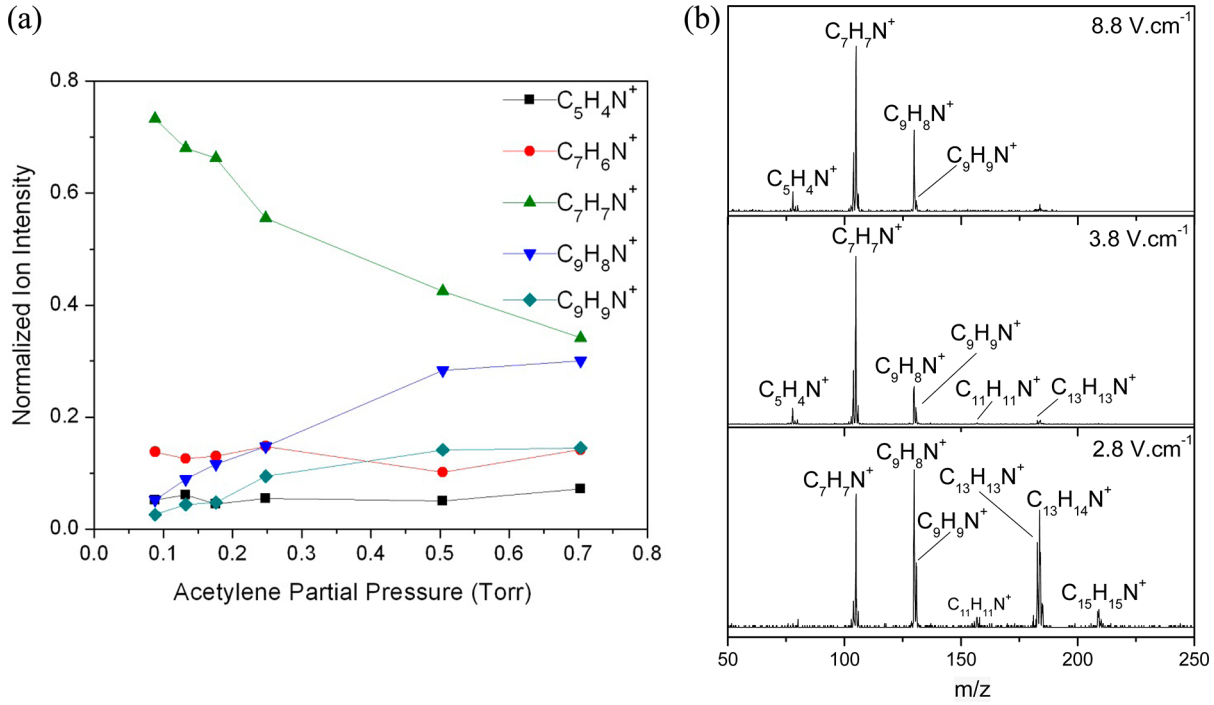

Figure 2. (a) Normalized ion intensity as a function of acetylene pressure in the drift cell in the presence of 0.70 Torr He at 303 K following the injection of the pyridinium ion into the drift cell. The injection energy used was 12.6 eV (lab frame), and the field across the cell was 5 V cm^{-1}. (b) Mass spectra obtained upon the injection of the mass-selected pyridinium ion ($C_5H_5N^{\bullet+}$) into the drift cell containing purified acetylene at 0.16 Torr at 314 K at different drift fields as indicated.

ions and branching ratios show no or weak dependence on the ion injection energy (Figure S2, Supporting Information).

The primary reactions observed at low concentration of acetylene at room temperature are listed below:

$$C_5H_5N^{\bullet+} + HCCH \rightarrow C_7H_7N^{\bullet+} \quad (3)$$

$$\rightarrow C_5H_4N^{+} + C_2H_3 \quad (4)$$

The even-electron $C_5H_4N^+$ ion produced by reaction 4 is known to be formed in the EI ionization of pyridine as a result of hydrogen loss from the meta position of the pyridinium ion.[64] However, in the present experiments when the mass-selected pyridinium ion is injected into the drift cell containing helium, no fragmentation is observed as shown in Figure 1a(i). Because the $C_5H_4N^+$ ion is only observed in the presence of acetylene, it is most likely formed by H abstraction by acetylene from the pyridinium ion as shown in reaction 4. This reaction is observed at early times probably as a result of a small fraction of unthermalized $C_5H_5N^{\bullet+}$ ions resulting from the ion injection process. The resulting $C_5H_4N^+$ ion and its association product with acetylene ($C_7H_6N^+$, m/z 104) do not react further with acetylene as indicated by the normalized ion intensity plots obtained at different concentrations of acetylene shown in Figure 2a. As the concentration of acetylene increases, the intensity of the first adduct $C_7H_7N^{\bullet+}$ (m/z 105) decreases and two parallel products are generated: the dehydrogenated second adduct $C_9H_8N^+$ (m/z 130) and the second adduct $C_9H_9N^{\bullet+}$ (m/z 131) as shown in Figure 2a and illustrated by reactions 5 and 6 below. However, the generation of the dehydrogenated second adduct $C_9H_8N^+$ appears to be more favorable because it is observed at a lower concentration of acetylene before a significant amount of $C_9H_9N^{\bullet+}$ ion is formed. This could reflect an extra stability of the $C_9H_8N^+$ (m/z 130) ion.

$$C_7H_7N^{\bullet+} + HCCH \rightarrow C_9H_8N^{+} + H \quad (5)$$

$$\rightarrow C_9H_9N^{\bullet+} \quad (6)$$

The time-dependent product distribution at 314 K is determined by changing the voltage gradient in the drift cell as shown in Figure 2b. By decreasing the voltage gradient in the drift cell (from 8.8 to 3.8 to 2.8 V/cm), the residence time of the injected pyridinium ions inside the drift cell increases, which results in increasing the product yield into the two parallel channels $C_9H_8N^+(HCCH)_n$ and $C_9H_9N^{\bullet+}(HCCH)_n$ with n = 1−3 as shown in Figure 2b.

The formation of higher order adduct ions from the sequential reactions of acetylene with the pyridinium ion is remarkable considering that no acetylene addition was observed on the benzene cation ($C_6H_6^{\bullet+}$) at room temperature.[49] This indicates that replacing a CH group in the aromatic ring (benzene cation) with a nitrogen atom (pyridinium ion) has a significant effect on enhancing the ring growth mechanism by increasing the reactivity of the ring toward the sequential addition of acetylene. The observed ions correspond to the general formulas $C_nH_nN^{\bullet+}$ and $C_nH_{n-1}N^+$ with n = 5, 7, 9, 11, 13, and 15. All of the observed reactions in the $C_5H_5N^{\bullet+}$ + HCCH system were confirmed in the $C_5D_5N^{\bullet+}$ + HCCH system.

To measure the second-order rate coefficient due only to the primary products, we injected the pyridinium ion ($C_5D_5N^{\bullet+}$, m/z 84) with low injection energy into the drift cell containing a small concentration of HCCH (0.017 Torr) in the presence of 0.32 Torr helium as a third body buffer gas. Under these conditions, no $C_5D_4N^+$ ions are formed as shown in the mass

dx.doi.org/10.1021/ja3068116 | J. Am. Chem. Soc. 2013, 135, 155−166

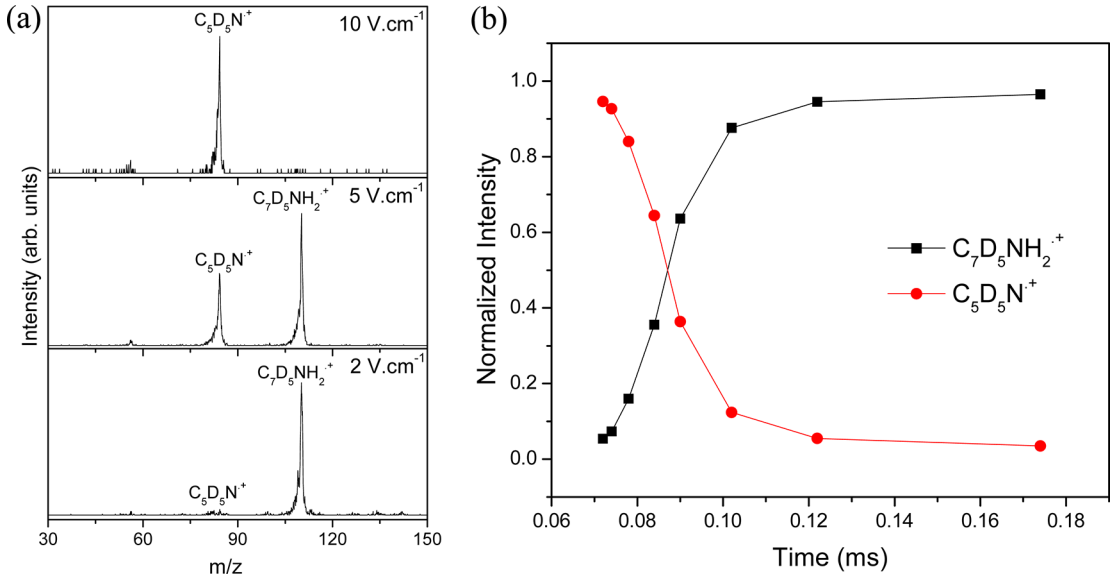

Figure 3. (a) Mass spectra obtained upon the injection of the mass-selected pyridinium ion ($C_5D_5N^{\bullet+}$) into the drift cell containing 0.017 Torr purified acetylene and 0.32 Torr He at 304 K at different drift fields as indicated. (b) Integrated arrival time distributions of the reactant ($C_5D_5N^{\bullet+}$) and product $C_7D_5NH_2^{\bullet+}$ ions as a function of reaction time for 0.017 Torr purified acetylene and 0.32 Torr He at 304 K.

spectra displayed in Figure 3a. At a higher drift field (10 V/cm) corresponding to a shorter residence time, only the $C_5D_5N^{\bullet+}$ ion is observed. As the drift field is decreased, the intensity of the pyridinium ion decreases, and at a drift field of 2 V/cm it reacts completely, generating the first adduct $C_7D_5NH_2^{\bullet+}$ (m/z 110) as shown in Figure 3a. The rate coefficient of 9.0($\pm$5.0) $\times$ 10^{-11} cm^3 s^{-1} at 304 K (Figure 3b, see Figure S3 for the pseudo first-order rate coefficient) measured by the current ion mobility technique reflects contributions from third body collisional stabilization by helium and acetylene. The rate coefficient shows no pressure dependence of the carrier gas within the measured range from 0.2 to 1.5 Torr helium, indicating that the reaction is second-order. The measured rate indicates a reaction efficiency (defined here as the ratio of the measured rate coefficient to the Langevin capture rate coefficient taken as 1.5 $\times$ 10^{-9} cm^3 s^{-1}) of nearly 6%, which is significant for the production of large organic ions in the gas phase. The high reactivity of the pyridinium ion toward acetylene is in sharp contrast to the very low reaction efficiency (10^{-4}) observed for the addition of acetylene on the benzene cation.[49] This confirms that the barrier to the aromatic cation ring growth can be overcome by substituting a ring carbon atom (CH) with a nitrogen atom.[52] Thus, nitrogen-containing complex organics can be produced by the sequential reactions of acetylene with ionized heterocyclic aromatics such as the pyridinium and pyrimidinium ions.

To compare the reactivity of the $C_5H_4N^{+}$ and $C_5H_5N^{\bullet+}$ toward the addition of acetylene and to confirm the covalent nature of the observed adduct ions, both ions were generated using higher injection energy of the pyridinium ion (24 eV, lab frame) and higher concentration of acetylene (1 Torr), and the product distribution was measured at both 311 and 623 K as shown in Figure 4a and b, respectively. Because of the higher injection energy and higher acetylene concentration used in these experiments, significant amounts of the $C_5H_4N^{+}$ and $C_5H_5NH^{+}$ (protonated pyridine) ions are produced as shown in Figure 4a. However, these ions appear to be unreactive toward acetylene as most of the observed product ions can be explained by the sequential reactions of acetylene with the

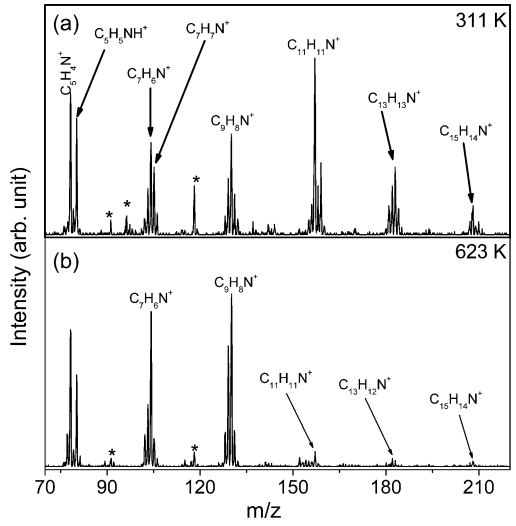

Figure 4. Mass spectra obtained upon the injection of the mass-selected pyridinium ion ($C_5H_5N^{\bullet+}$) into the drift cell containing purified acetylene at 1.0 Torr and different temperatures as indicated. The peaks marked with "*" are impurity peaks containing water and acetone due to the use of high concentration of acetylene.

$C_5H_5N^{\bullet+}$ ion generating the $C_nH_nN^{\bullet+}$ and $C_nH_{n-1}N^{+}$ ions with n up to 15 as shown in Figure 4a. At 623 K, the intensity of the higher adducts significantly decreases, suggesting thermal dissociation to generate the stable even-electron $C_7H_6N^{+}$ and $C_9H_8N^{+}$ ions as shown in Figure 4b. Alternatively, this could be due to unimolecular dissociation in the formation step of the weakly bound ions, which could reflect weaker sequential binding energies. It is interesting to note that the $C_9H_8N^{+}$ ion (m/z 130) that could correspond to the quinolizinium cation appears to be the major product formed from the sequential reactions of acetylene with the pyridinium ion at higher temperatures. Possible structures of the pyridinium ion–acetylene adducts are investigated by ion mobility, ion dissociation, and DFT calculations in the next sections.

dx.doi.org/10.1021/ja3068116 | J. Am. Chem. Soc. 2013, 135, 155–166

2. Intracluster Reactions of Ionized Pyridine–Acetylene Binary Clusters. In the gas phase at low pressures, ion–molecule reactions may proceed via an elimination mechanism.[59,65,66] However, in the same systems at high pressure, the ionic intermediates may be stabilized, and addition without elimination may occur. In clusters, both elimination and addition reactions can take place resulting in product ion distributions that reflect both the stability of the covalent adducts and the kinetics of the reactions.[56,57,59,67−72] Therefore, sequential polymerization and growth involving several addition and/or elimination steps can occur following the ionization of isolated molecular clusters.[56,57,59,67−72] This occurs because the energy released from the condensation reactions can be efficiently dissipated by fast evaporation (boiling off) of nonreacting monomers from the cluster. The competition between the condensation reactions leading to the growth of the covalent ion and monomer evaporation resulting in depleting the monomer concentration in the cluster can control the ultimate size that the covalent ion can reach in the cluster.

To study the intracluster reactions, we generated $(\text{pyridine})_n$-$(\text{acetylene})_m$ binary clusters using the supersonic beam expansion technique.[56,59,67−72] One of the major questions that must be addressed is whether the resulting ions are covalent adducts formed by intracluster reactions, or simply cluster ions held together by electrostatic ion-induced dipole forces. To answer this question, we used a combination of ion dissociation and ion mobility measurements assisted by DFT structural calculations of possible product ions as described below.

A typical mass spectrum of the EI-ionized pyridine–acetylene binary clusters is shown in Figure 5. In addition to the acetylene cluster ions $(A)_n^{\bullet+}$ with n = 2−5, the spectrum shows the $C_5D_5N(C_2H_2)_n$ series $(PyA_n)^{\bullet+}$ with n = 1−4 and a very intense peak corresponding to the cluster ion (Py_2A) consisting of one acetylene and two pyridine molecules [possibly $(C_5D_5N)^{\bullet+}(C_2H_2)(C_5D_5N)$]. This ion shows a strong enhanced intensity (magic number behavior) under different experimental conditions suggesting a special stability, probably due to the high binding energy of a geometrically stable structure. Furthermore, a protonated pyridine dimer (Py_2H^+) representing $(C_5D_5N)_2H^+$ is observed and appears to be formed through the loss of a $C_2H^\bullet$ radical from the $[(C_5D_5N)(C_2H_2)(C_5D_5N)]^{\bullet+}$ ion.

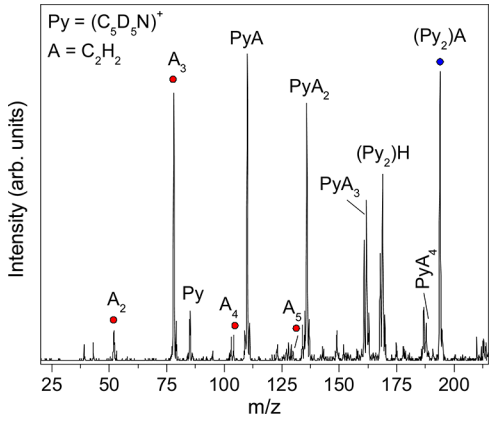

Figure 5. Mass spectrum of the EI-ionized pyridine (Py, C_5D_5N)/acetylene (A, C_2H_2) binary clusters formed by supersonic beam expansion and injected into the drift cell containing 0.5 Torr He at 303 K.

The mass-selected ions can be efficiently dissociated by gradually increasing the injection energy of the ions into the drift cell, and the dissociated products can provide structural information. To obtain such information, we measured the dissociation products of the $C_7D_5H_2N^{\bullet+}$ and $(C_5D_5N)_2(C_2H_2)^{\bullet+}$ ions by increasing the injection energies of the mass-selected ions into the drift cell containing a helium buffer gas. As shown in Figure 6a, no dissociation products of the mass-selected $C_7D_5H_2N^{\bullet+}$ ions are observed until the IE is increased above 23 eV (lab frame) consistent with the covalent bonding nature of these ions. The major dissociation channel involves a loss of the C_2H_2 unit to generate the $C_5D_5N^{\bullet+}$ ion consistent with the direct attachment of the acetylene molecule to the nitrogen site of the pyridinium ion. If C_2H_2 is attached to a carbon site of the pyridinium ion, then the loss of C_2DH_2 should generate the $C_5D_4N^+$ ion, which is not observed. Furthermore, the observed loss of a hydrogen atom from the $C_7D_5H_2N^{\bullet+}$ ion at higher injection energies (30−40 eV, Figure 6a) suggests that the C_2H_2 unit is attached covalently to the nitrogen site of the pyridinium ion.

The dissociation products of the Py_2A ion at higher injection energies, shown in Figure 6b, indicate that the major dissociation channel involves a loss of a pyridine unit (C_5D_5N) to generate the $C_7D_5H_2N^{\bullet+}$ ion consistent with the C_2H_2 unit being attached to the two nitrogen sites of the two pyridine molecules. The stability of the $C_7D_5H_2N^{\bullet+}$ ion is also suggested by the lack of dissociation into the pyridinium ion ($C_5D_5N^{\bullet+}$) even at very high injection energies such as 52 eV as shown in Figure 6b.

To further support the proposed structures based on the injection energies experiments, we measured the mobility of the $C_7D_5H_2N^{\bullet+}$ and $C_9D_5H_4N^{\bullet+}$ ions (m/z 110 and 136, respectively) as well as of the remarkably stable $(C_5D_5N)_2(C_2H_2)^{\bullet+}$ ion (m/z 194) produced in the ionized pyridine–acetylene binary clusters. Ion mobility measurements provide an accurate method for determining collision cross sections of mass-selected ions in a buffer gas.[56,60,73−76] The motion of the ion through a buffer gas under the influence of a weak electric field depends on the ion's average collision cross section (collision integral, Ω) with the buffer gas, which depends on the geometric shape of the ion.[56,60,73−76] Theoretical calculations of possible structural candidates of the mass-selected ions are then used to compute angle-averaged Ω's at different temperatures for comparison with the measured ones.[56,60,73−76]

The ion mobility measurements (see Figures S4–S6, Supporting Information) yield collision cross sections (in helium at 305 K) for the $C_7D_5H_2N^{\bullet+}$, $C_9D_5H_4N^{\bullet+}$, and $(C_5D_5N)_2(C_2H_2)^{\bullet+}$ ions as 56.3 ± 1.9, 65.9 ± 2.8, and 82.4 ± 2.7 Å^2, respectively.

The low energy structures of the $C_7H_7N^{\bullet+}$, $C_9H_9N^{\bullet+}$, and $(C_5H_5N)_2(C_2H_2)^{\bullet+}$ ions and their relative energies calculated at the B3LYP/6-31G* level along with their calculated Ωs using the trajectory method[63] are shown in Figures 7, 8, and 9, respectively. Figure 7 shows the six lowest energy covalent bonded structures (1−6) of the $C_7H_7N^{\bullet+}$ ion in addition to two ion–molecule structures (7 and 8). It is clear that the noncovalent higher energy ion–molecule structures (7 and 8) can be excluded on the basis of the mobility measurements because they have collisional cross sections significantly larger than the measured Ω values. More important, the ion–molecule structures are not consistent with the high temperature and ion dissociation experiments, which confirm the covalent bonding nature of the observed pyridinium ion–acetylene adducts. However, all of the six lowest energy

dx.doi.org/10.1021/ja3068116 | J. Am. Chem. Soc. 2013, 135, 155−166

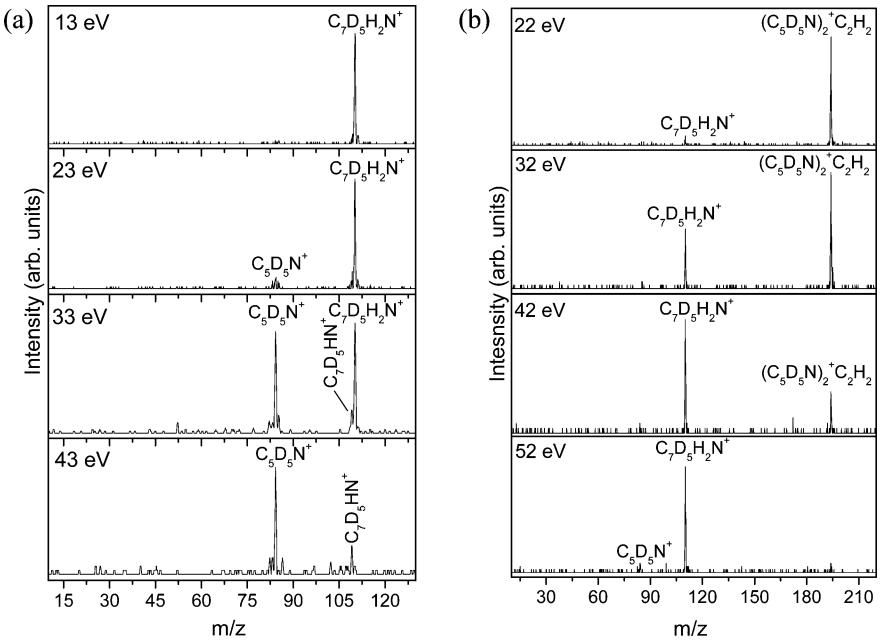

Figure 6. (a) Mass spectra of the mass-selected pyridine (Py, C_5D_5N)/acetylene (A, C_2H_2) binary cluster ($PyA^{\bullet+}$, m/z 110) upon injection into the drift cell containing 0.7 Torr He at 303 K using different injection energies (lab frame) as indicated. (b) Mass spectra of the mass-selected $Py_2A^{\bullet+}$ binary cluster [$(C_5D_5N)_2C_2H_2^{\bullet+}$, m/z 194] upon injection into the drift cell containing 0.4 Torr He at 305 K using different injection energies (lab frame) as indicated.

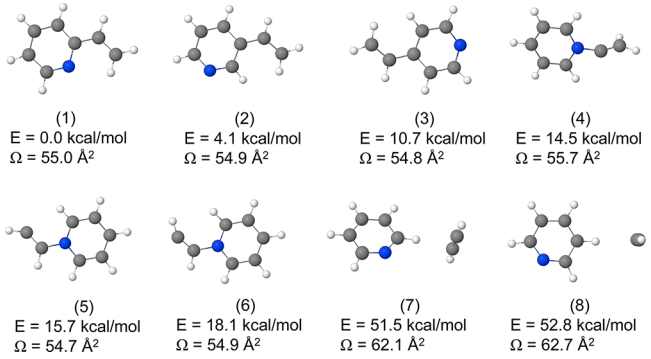

Figure 7. Relative energies (E) of the lowest energy structures of the $C_7H_7N^{\bullet+}$ ion calculated at the B3LYP/6-31G* level of theory. The collision cross sections (Ω) were calculated at 305 K using the trajectory method and Mobcal program (ref 63). The measured Ω of the $C_7D_5H_2N^{\bullet+}$ ion (m/z 110) in 2.16 Torr He at 305 K is 56.3 ± 1.9 Å^2.

covalent isomers of the $C_7H_7N^{\bullet+}$ ion shown in Figure 7 have Ω values similar to the experimental value of 56.3 ± 1.9 Å^2. Therefore, mobility measurements alone may not be able to distinguish between different covalent isomers with similar structures. On the other hand, the ion dissociation experiment supports only structures (4), (5), and (6) because the reaction site appears to be N, not C. In fact, structure (5) has been predicted to be the most favorable $C_7H_7N^{\bullet+}$ product that can form from the reaction of pyridinium ion and acetylene.[52] The reaction was found to be exothermic by 44.3 kcal/mol (at the B3LYP/6-31G* level), and the addition of acetylene to the nitrogen atom occurs without a barrier (−14.4 kcal/mol).[52] Although the CHCH side group of structure (5) can rearrange to C═CH_2 as in the lower energy structure (4), the barrier for the intramolecular 1,2 H migration was found to be 49.7 kcal/mol so this process was considered unfavorable.[52] Therefore, on the basis of the combination of the high temperature, ion dissociation, and mobility experiments supported by the DFT structures and the previous reaction pathway calculations,[52] we conclude that the structure of the $C_7H_7N^{\bullet+}$ ion observed in our experiments is structure (5).

Figure 8 displays the six lowest energy covalent bonded structures (a–f) of the $C_9H_9N^{\bullet+}$ ion in addition to six ion–molecule structures (g–l). Again, the high energy ion–molecule structures (g–l) are not consistent with the combination of high temperature, ion dissociation, and mobility experiments, and therefore these structures can be excluded. Furthermore, the four lowest energy covalent structures of the $C_9H_9N^{\bullet+}$ ion (a–d) do not include the pyridinium ion structure and require extensive high energy rearrangements to be produced, which are unlikely to take place under the conditions of our experiments. Therefore, it appears that structure (e) (Figure 8e) is the only structure consistent with the experimental results and also with the structural assignment of the reactant $C_7H_7N^{\bullet+}$ ion (Figure 7, structure 5).

Structure (e) (Figure 8) has been predicted to result from the addition of a second acetylene molecule to the $C_7H_7N^{\bullet+}$ ion (structure 5) in a barrierless (−1.8 kcal/mol) and exothermic (−44.5 kcal/mol) process.[52] The formation of structures (5) and (e) corresponding to the observed first $C_7H_7N^{\bullet+}$ (m/z 105) and second $C_9H_9N^{\bullet+}$ (m/z 131) adducts, respectively, is shown in reactions 7 and 8, respectively.

It is interesting to note that the dehydrogenated second adduct $C_9H_8N^+$ (m/z 130) was formed in our experiments in parallel with the second adduct $C_9H_9N^{\bullet+}$ at room temperature (Figures 1a,b and 2a), and it was the major ion formed at 623 K as shown in Figure 4b. The formation of a bicyclic ion *c*-(e) shown in reaction 9 by the closure of the second ring of structure (e) was found to be exothermic by 34.6 kcal/mol and to involve only a very small barrier of 1.4 kcal/mol.[52] On the other hand, the loss of the extra H atom from the bicyclic ion *c*-(e) to form the quinolizinium cation as shown in reaction 9 was found to be endothermic by 9.5 kcal/mol, and to involve a barrier.[52] However, if the ring closure of (e) occurs in conjunction

dx.doi.org/10.1021/ja3068116 | J. Am. Chem. Soc. 2013, 135, 155–166

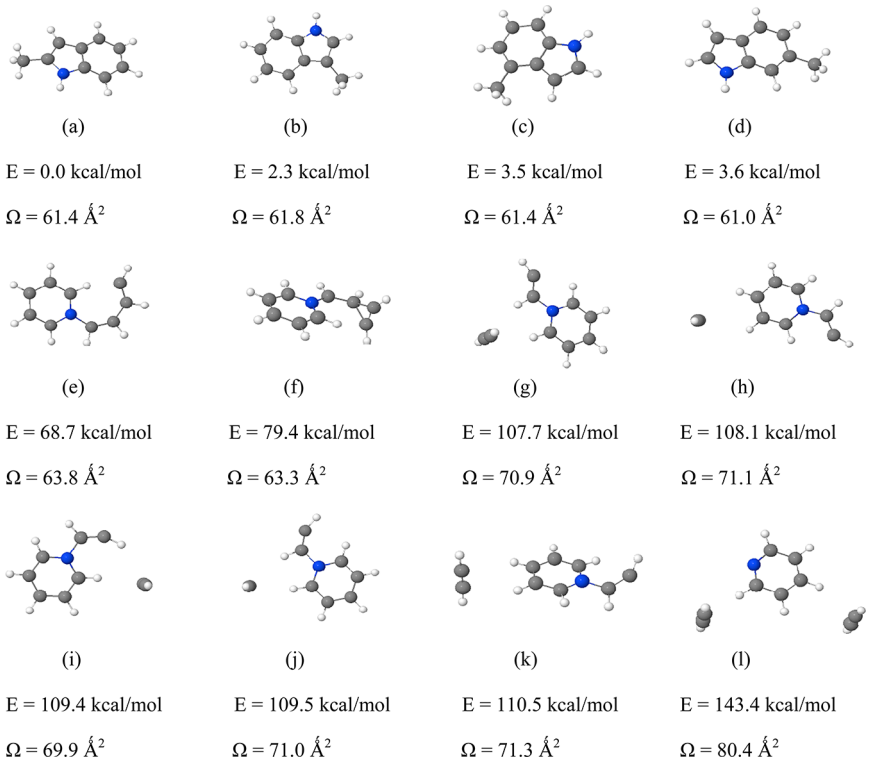

Figure 8. Relative energies (E) of the lowest energy structures of the $C_9H_9N^{\bullet+}$ ion calculated at the B3LYP/6-31G* level of theory. The collision cross sections (Ω) were calculated at 304 K using the trajectory method and Mobcal program (ref 63). The measured Ω for the $C_9D_5H_4N^{\bullet+}$ ion (m/z 136) in 2.33 Torr He at 305 K is 65.9 ± 2.8 Å^2.

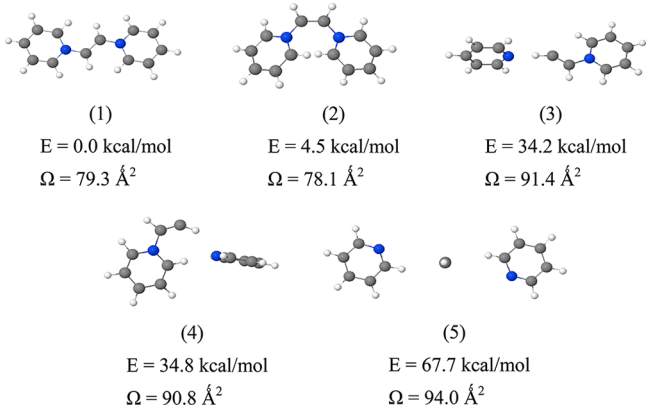

Figure 9. Relative energies (E) of the lowest energy structures of the $(C_5H_5N)_2C_2H_2^{\bullet+}$ cluster ion calculated at the B3LYP/6-31G* level of theory. The collision cross sections (Ω) were calculated at 306 K using the trajectory method and Mobcal program (ref 63). The measured Ω for the $(C_5D_5N)_2C_2H_2^{\bullet+}$ ion (m/z 194) in 3.52 Torr He at 306 K is 82.4 ± 2.7 Å^2.

(or concerted) with the H atom loss, then the overall reaction 9 becomes exothermic by at least 25 kcal/mol.[52] In fact, the addition/H-elimination reaction of acetylene and the first adduct $C_7H_7N^{\bullet+}$ having structure (1), (2), (3), (4), or (5) (shown in Figure 7) (reaction 5) is exothermic by 65.9, 61.8, 55.2, 51.4, or 50.2 kcal/mol, respectively, at the B3LYP/6-31G* level. Therefore, the structure of the dehydrogenated second adduct $C_9H_8N^+$ formed in our experiments is likely to be the bicyclic quinolizinium cation shown in reaction 9.

The calculated structures of the $(C_5D_5N)_2(C_2H_2)^{\bullet+}$ ion, shown in Figure 9, result in two covalent bonded (1 and 2) and three higher energy ion−molecule complexes (3−5). As

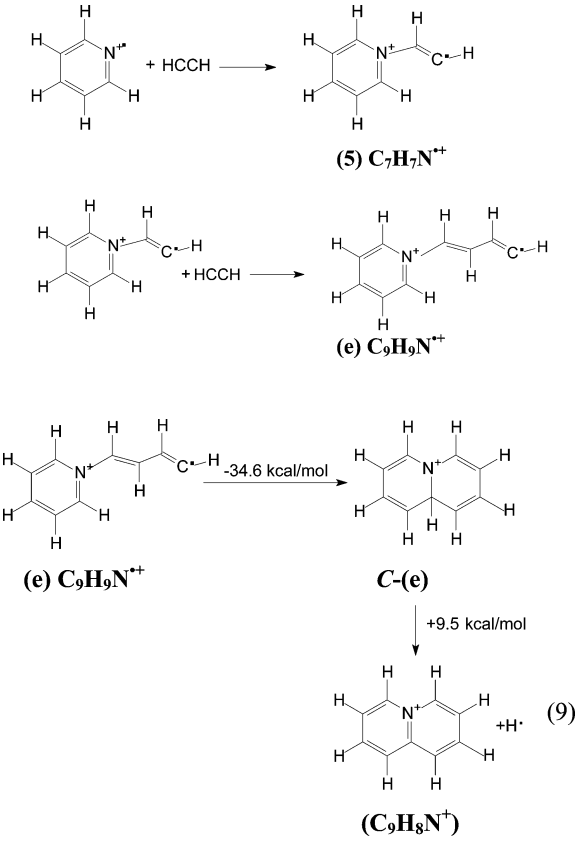

expected, the ion−molecule structures have collision cross sections significantly larger (91−94 Å^2) than the measured Ω value (82.4 ± 2.7 Å^2). Both of the covalent structures are

dx.doi.org/10.1021/ja3068116 | J. Am. Chem. Soc. 2013, 135, 155−166

consistent with the ion dissociation and mobility measurements, and therefore these structures are tentatively assigned to the observed $(C_5D_5N)_2(C_2H_2)^{\bullet+}$ ion. These structures show that the growth of the $C_7H_7N^{\bullet+}$ ion can be terminated by a second pyridine molecule. These structures (1 and 2 in Figure 9) also explain the observed magic number behavior of the $(C_5D_5N)_2(C_2H_2)^{\bullet+}$ ion shown in Figure 5.

3. Gas-Phase Reactions of Acetylene with the Pyrimidinium Ion. For comparison with the pyridinium ion results, the reactions of acetylene with the pyrimidinium ion ($C_4H_4N_2^{\bullet+}$) were investigated. Figure 10 displays the mass spectra obtained following the injection of the mass-selected pyrimidinium ion into the drift cell containing 1.2−1.6 Torr helium and different amounts of acetylene at room temperature. As expected, only the parent ion $C_4H_4N_2^{\bullet+}$ is observed in pure helium (Figure 10a), indicating the absence of pyrimidine fragments or impurity ions in the drift cell. In the presence of a very low concentration of acetylene (4×10^{-5} Torr), the formation of first adduct $C_6H_6N_2^{\bullet+}$ is observed (Figure 10b) followed by the dehydrogenated second adduct $C_8H_7N_2^+$ when the partial pressure of acetylene is increased to 0.03 Torr (Figure 10c). Similar to the reactions with the pyridinium ion, a dehydrogenated second acetylene adduct is observed. However, in the pyrimidinium ion reactions, the dehydrogenated product is the only second adduct observed because the $C_8H_8N_2^{\bullet+}$ ion is not observed even at higher concentrations of acetylene as shown in Figure 10d−f. As the concentration of acetylene is increased, the intensity of the even-electron ion $C_8H_7N_2^+$ increases, and the first adduct is completely converted into the $C_8H_7N_2^+$ ion as shown in Figure 10f in the presence of 1.3 Torr pure acetylene. A small signal corresponding to an ion with m/z 78 is also observed under higher concentrations of acetylene as shown in Figure 10e and f. The presence of impurity can be excluded because no m/z 78 ion is observed when the pyrimidinium ion is injected into pure helium as shown in Figure 10a. This ion could be $C_6H_6^{\bullet+}$ formed by dissociative charge transfer reaction of the $C_4H_4N_2^{\bullet+}(C_2H_2)_3$ ion where partial charge transfer from the pyrimidinium ion (IE = 9.3 eV) to the acetylene trimer activates the formation of a benzene cation (IE = 9.2 eV) and ejection of a pyrimidine neutral. In this case, dissociative charge transfer occurs before collisional stabilization of the associated $C_4H_4N_2^{\bullet+}(C_2H_2)_3$ ion, and as a result the corresponding m/z 158 ion is not observed. A similar process has been previously observed at low temperatures when a large number of acetylene molecules is associated with a benzene cation.[49,50]

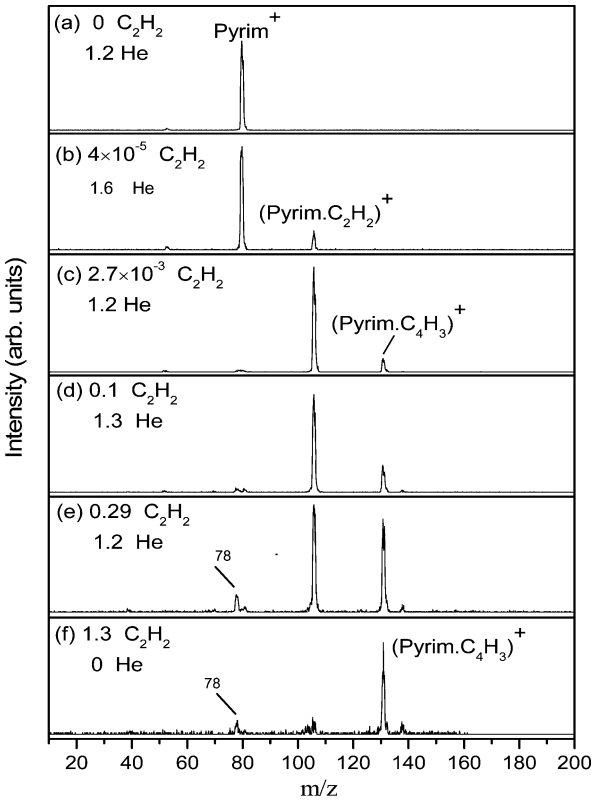

Figure 10. Mass spectra obtained upon the injection of the mass-selected pyrimidinium ion ($C_4H_4N_2^{\bullet+}$, m/z 80) into the drift cell containing purified acetylene and helium at different partial pressures (Torr) as indicated at 304 K.

The high reactivity of acetylene toward the pyrimidinium ion is illustrated in Figure 11a, which shows that at longer reaction times, the pyrimidinium ion reacts almost completely with acetylene even at a very low partial pressure of acetylene of 5×10^{-4} Torr. Indeed, the disappearance of $C_4H_4N_2^{\bullet+}$ ions (m/z 80) and the formation of the first adduct ($C_6H_6N_2^{\bullet+}$, m/z 106) and the dehydrogenated second adduct ($C_8H_7N_2^+$, m/z 131) occurs at nearly the collision rate with a measured rate coefficient of $1.4(\pm 1.2) \times 10^{-9}$ cm^3 s^{-1} at 308 K as shown in Figure 11b (see Figure S7 for the first-order rate coefficient). The rate coefficient shows no dependence on the helium pressure within the investigated range from 0.3 to 1.6 Torr, indicating that the reaction is second-order. The thermal stability of the adduct ions $C_6H_6N_2^{\bullet+}$ and $C_8H_7N_2^+$ is demonstrated by the lack of observed thermal dissociation at nearly 500 K (Figure S8, Supporting Information), thus confirming the covalent bonding nature of these ions.

The calculated low energy structures of the $C_6H_6N_2^{\bullet+}$ and $C_8H_7N_2^+$ ions and their relative energies at the B3LYP/6-31G* level are shown in Figure 12. It is interesting to note that the addition of the second acetylene molecule to the lowest energy structure of the $C_6H_6N_2^{\bullet+}$ adduct (structure (a), Figure 12A) followed by a hydrogen loss leads to the formation of the second adduct $C_8H_7N_2^+$ which is the lowest energy structure of the pyrido[1,2-α] pyrimidinium cation (structure (a), Figure 12B). The observed 100% reaction efficiency of acetylene with the pyrimidinium ion is consistent with the trend of increasing reaction rate with the substitution of CH groups with nitrogen atoms in the aromatic ring. This implies that cyclic ions containing multiple nitrogen atoms that could be formed by sequential reactions of HCN with acetylene ions could lead to the growth of large nitrogen-containing PAHs under appropriate astrochemical conditions.

Trends in Reaction Rates of Ionized Aromatics with Acetylene. The measured rate coefficients of the acetylene reactions with the pyridinium and pyrimidinium ions reveal a clear trend in the reactivity of acetylene with ionized aromatics to form larger covalent ions. For example, acetylene does not react with the benzene radical cation at room temperature, and even the associated $C_6D_6^{\bullet+}(C_2H_2)_n$ products are not observed due to weak binding.[49,50] However, sequential reactions of acetylene with the benzene radical cation are observed at higher temperatures (600 K) leading to the formation of naphthalene-type ions.[49] The barrier to the covalent addition of acetylene onto the benzene radical cation ($C_6H_6^{\bullet+}$) originates from the presence of six C−H bonds in the benzene cation and the

dx.doi.org/10.1021/ja3068116 | J. Am. Chem. Soc. 2013, 135, 155−166

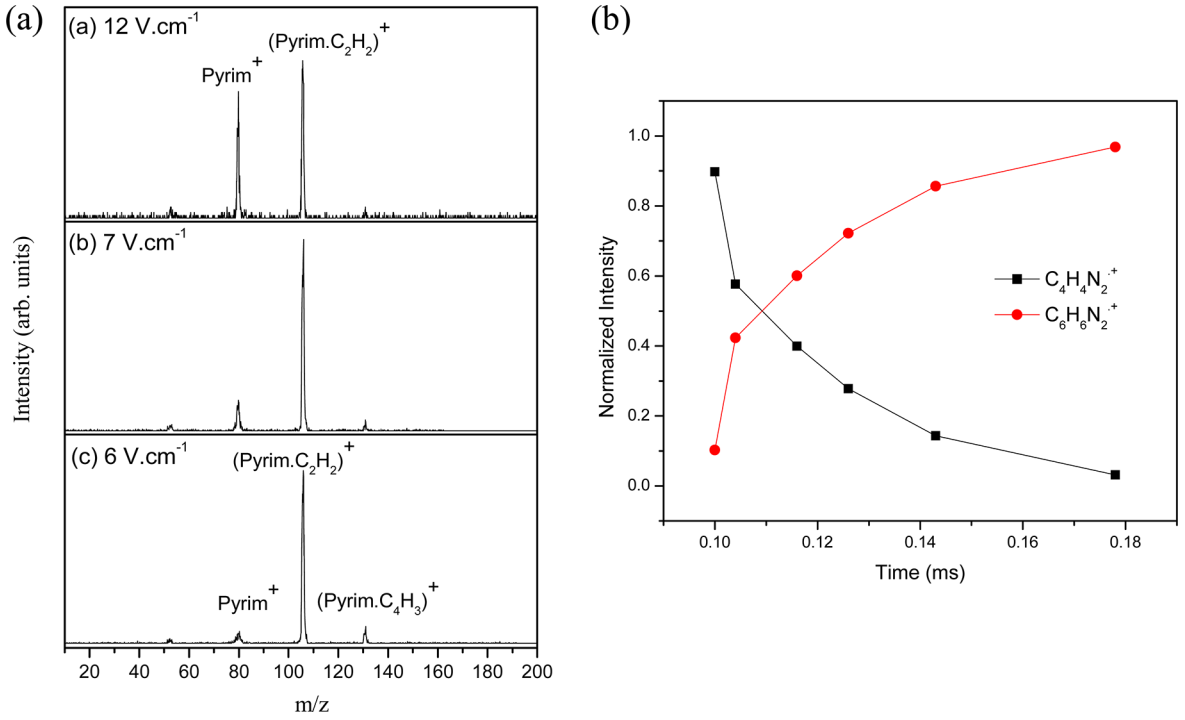

Figure 11. (a) Mass spectra obtained upon the injection of the mass-selected pyrimidinium ion ($C_4H_4N_2^{\bullet+}$, m/z 80) into the drift cell containing 0.053 Torr of a 1% acetylene in helium mixture and 1.55 Torr He at 301 K at different drift fields as indicated. (b) Integrated arrival time distributions of the reactant pyrimidinium ion ($C_4H_4N_2^{\bullet+}$, m/z 80) and product pyrim·$C_2H_2^{\bullet+}$ ($C_6H_6N_2^{\bullet+}$, m/z 106) as a function of reaction time. The mass-selected pyrimidinium ion was injected into the drift cell containing 3×10^{-4} Torr acetylene and 1.55 Torr helium at 308 K.

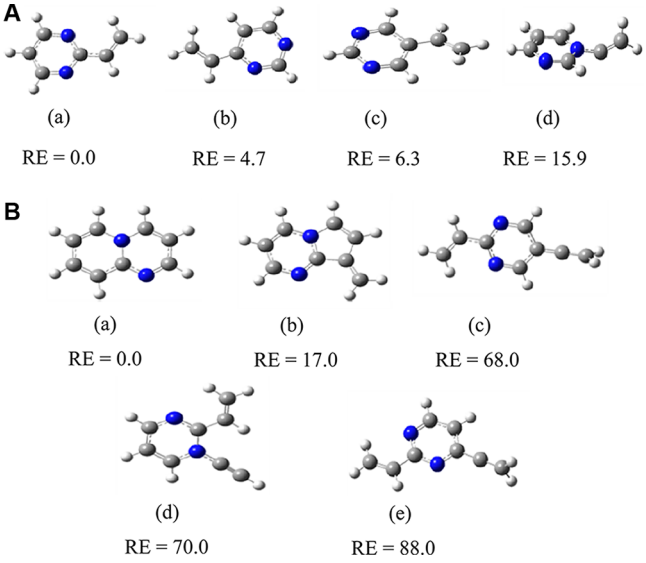

Figure 12. (A) Relative energies (RE, kcal/mol) of the lowest energy structures of the $C_6H_6N_2^{\bullet+}$ ion calculated at the B3LYP/6-31G* level of theory. (B) Relative energies (RE, kcal/mol) of the lowest energy structures of the $C_8H_7N_2^{+}$ ion calculated at the B3LYP/6-31G* level of theory.

absence of an available addition site.[51−53] This is confirmed in the recent measurement of the high reactivity of acetylene toward the phenylium ion to generate the covalent adduct $C_8H_7^+$ with a reaction efficiency of nearly 35−47% at room temperature.[58] In the present experiments, the reaction efficiencies of acetylene with the pyridinium and pyrimidinium ions at room temperature are found to be 6% and 100%, respectively. Therefore, the observed trend suggests that substitution of a ring carbon atom (CH) in the benzene cation with a nitrogen atom enhances the aromatic cation ring growth mechanism by the addition of acetylene. However, this enhancement is more pronounced if a hydrogen atom is removed from the benzene ring as in the phenylium ion, and the ultimate enhancement occurs when two ring carbon atoms are replaced by nitrogen atoms as in the pyrimidinium ion. Thus, nitrogen-containing complex organics can be readily produced by the sequential reactions of acetylene with ionized heterocyclic aromatics containing multiple nitrogen atoms.

SUMMARY AND CONCLUSIONS

In this work, we present the first direct experimental evidence for the formation of nitrogen-containing complex organic ions by sequential reactions of acetylene with the pyridinium and pyrimidinium ions in the gas phase and within ionized pyridine−acetylene binary clusters. Additions of five and two acetylene molecules onto the pyridinium and pyrimidinium ions, respectively, at room temperature are observed. Second-order rate coefficients of the overall reaction of acetylene with the pyridinium and pyrimidinium ions are measured as 9.0×10^{-11} and 1.4×10^{-9} cm^3 s^{-1}, respectively, indicating reaction efficiencies of about 6% and 100%, respectively, at room temperature. At high temperatures, only two acetylene molecules are added to the pyridinium and pyrimidinium ions, suggesting covalent bond formation. A combination of ion dissociation and ion mobility experiments with DFT calculations reveals that the addition of acetylene into the pyridine cation occurs through the N-atom of the pyridinium ion. The relatively high reaction efficiency is consistent with the absence of a barrier in the exothermic N−C bond forming reaction leading to the formation of the $C_7H_7N^{\bullet+}$ covalent adduct. An

dx.doi.org/10.1021/ja3068116 | J. Am. Chem. Soc. 2013, 135, 155−166

exothermic addition/H-elimination reaction channel of acetylene onto the $C_7H_7N^{\bullet+}$ adduct is observed leading to the formation of a bicyclic quinolizinium cation. Similar chemistry is observed in the sequential reactions of acetylene with the pyrimidinium ion. The second acetylene addition onto the pyrimidinium ion involves an exclusive loss of H atom at room temperature, suggesting the formation of a bicyclic pyrimidinium cation ($C_8H_7N_2^+$). The high reactivity of the pyridinium and pyrimidinium ions toward acetylene is in sharp contrast to the very low reactivity of the benzene cation, which has a reaction efficiency of 10^{-4}–10^{-5}. This indicates that the presence of a nitrogen atom within the aromatic ring enhances the ring growth mechanism by the sequential addition of acetylene to form nitrogen-containing polycyclic hydrocarbon ions. The observed reactions may explain the possible formation of nitrogen-containing complex organics by gas-phase ion–molecule reactions involving the pyridinium and pyrimidinium ions with acetylene under a wide range of temperatures and pressures in astrochemical environments such as the nitrogen-rich Titan's atmosphere. However, it should be stated that this mechanism requires ion neutralization as a final step. Further studies are needed on the neutralization reactions of large nitrogen-containing radical cations before searching for spectroscopic evidence for these organics in Titan's atmosphere can be suggested.

■ ASSOCIATED CONTENT

Supporting Information

(S1) Schematic diagram of the mass-selected ion mobility tandem mass spectrometer at VCU, (S2) normalized ion intensity of the product ions as a function of the injection energy of the pyridinium ion into acetylene–helium mixture, (S3) kinetic plot to determine the pseudo first-order rate coefficient for the reaction of $C_5D_5N^{\bullet+}$ with acetylene, measured arrival time distributions (ATDs) used to calculate the reduced mobilities and collision cross sections (in helium) of the mass-selected $C_7D_5H_2N^{\bullet+}$(S4), $C_9D_5H_4N^{\bullet+}$ (S5), $(C_5D_5N)_2(C_2H_2)^{\bullet+}$ (S6) ions produced by EI ionization of the pyridine–acetylene binary clusters, (S7) kinetic plot to determine the pseudo first-order rate coefficient for the reaction of $C_5H_4N_2^{\cdot+}$ with acetylene, and (S8) mass spectra obtained upon the injection of the pyrimidinium ion into the drift cell containing acetylene–helium mixture at different temperatures (322, 440, and 494 K). This material is available free of charge via the Internet at http://pubs.acs.org.

■ AUTHOR INFORMATION

Corresponding Author

mselshal@vcu.edu

Notes

The authors declare no competing financial interest.

■ ACKNOWLEDGMENTS

We thank Dr. Ridha Mabrouki, Washington River Protection Solutions, Richland, WA, for assistance with some of the early measurements of the pyridinium ion–acetylene reactions. We also thank Prof. Samuel Abrash, University of Richmond, Richmond, VA, for assistance with some of the DFT calculations. This work was supported by the National Science Foundation Grant CHE-0911146 and NASA Grant NNX08AI46G.

■ REFERENCES

(1) Kress, M. E.; Tielens, A. G. G. M.; Freklach, M. *Adv. Space Res.* **2010**, *46*, 44–49.
(2) Herbst, E.; van Dishoeck, E. F. *Annu. Rev. Astron. Astrophys.* **2009**, *47*, 427–80.
(3) Tielens, A. G. G. M. *Ann. Rev. Astron. Astrophys.* **2008**, *46*, 289–337.
(4) Waite, J. H., Jr.; Young, D. T.; Cravens, T. E.; Coates, A. J.; Crary, F. J.; Magee, B.; Westlake, J. *Science* **2007**, *316*, 870–875.
(5) Robinson, A. L.; Donahue, N. M.; Shrivastava, M. K.; Weitkamp, E. A.; Sage, A. M.; Grieshop, A. P.; Lane, T. E.; Pierce, J. R.; Pandis, S. N. *Science* **2007**, *315*, 1259–1262.
(6) Duley, W. W. *Faraday Discuss.* **2006**, *133*, 415–425.
(7) Sandford, S. A.; Aléon, J.; Alexander, C. M. O'D.; Araki, T.; Bajt, S.; Baratta, G. A.; Borg, J.; Bradley, J. P.; Brownlee, D. E.; Brucato, J. R.; Burchell, M. J.; Busemann, H.; Butterworth, A.; Clemett, S. J.; Cody, G.; Colangeli, L.; Cooper, G.; D'Hendecourt, L.; Djouadi, Z.; Dworkin, J. P.; Ferrini, G.; Fleckenstein, H.; Flynn, G. J.; Franchi, I. A.; Fries, M.; Gilles, M. K.; Glavin, D. P.; Gounelle, M.; Grossemy, F.; Jacobsen, C.; Keller, L. P.; Kilcoyne, A. L. D.; Leitner, J.; Matrajt, G.; Meibom, A.; Mennella, V.; Mostefaoui, S.; Nittler, L. R.; Palumbo, M. E.; Papanastassiou, D. A.; Robert, F.; Rotundi, A.; Snead, C. J.; Spencer, M. K.; Stadermann, F. J.; Steele, A.; Stephan, T.; Tsou, P.; Tyliszczak, P. T.; Westphal, A. J.; Wirick, S.; Wopenka, B.; Yabuta, H.; Zare, R. N.; Zolensky, M. E. *Science* **2006**, *314*, 1720–1724.
(8) Niemann, H. B.; Atreya, S. K.; Bauer, S. J.; Carignan, G. R.; Demick, J. E.; Frost, R. L.; Gautier, D.; Haberman, J. A.; Harpold, D. N.; Hunten, D. M.; Israel, G.; Lunine, J. I.; Kasprzak, W. T.; Owen, T. C.; Paulkovich, M.; Raulin, F.; Raaen, E.; Way, S. H. *Nature* **2005**, *438*, 779–784.
(9) Ehrenfreund, P.; Sephton, M. A. *Faraday Discuss.* **2006**, *133*, 277–288.
(10) Xu, X.; Pacey, P. *Phys. Chem. Chem. Phys.* **2005**, *7*, 326–333.
(11) Richter, H.; Howard, J. B. *Phys. Chem. Chem. Phys.* **2002**, *4*, 2038–2055.
(12) Saha, B.; Irle, S.; Morokuma, K. J. *Chem. Phys.* **2010**, *132*, 224303–224314.
(13) Cernicharo, J.; Heras, M.; Tielens, A. G. G. M.; Pardo, J. R.; Herpin, F.; Guelin, M.; Waters, L. B. F. M. *Astrophys. J.* **2001**, *546*, L123–L126.
(14) Winnewisser, G.; Kramer, C. *Space Sci. Rev.* **1999**, *90*, 181–202.
(15) Calcote, H. F.; Keil, D. G. *Pure Appl. Chem.* **1990**, *62*, 815–824.
(16) Shock, E. L.; Shulte, M. D. *Nature* **1990**, *343*, 728–731.
(17) Chyba, C. F.; Sagan, C. *Nature* **1992**, *335*, 125–132.
(18) Strazzulla, G.; Baratta, G. A.; Spinella, F. *Adv. Space Res.* **1995**, *15*, 385–400.
(19) Salama, F.; Joblin, C.; Allamandola, L. J. *Planet. Space Sci.* **1995**, *43*, 1165–1173.
(20) Brooke, T. Y.; Tokunaga, A. T.; Weaver, H. A.; Crovisier, J.; Bockelee-Morvan, D.; Crisp, D. *Nature* **1996**, *383*, 606–607.
(21) Weilmünster, P.; Keller, A.; Homann, K.-H. *Combust. Flame* **1999**, *116*, 62–83.
(22) Frenklach, M. *Phys. Chem. Chem. Phys.* **2002**, *4*, 2028–2037.
(23) Woods, P. M.; Millar, T. J.; Zijlstra, A. A.; Herbst, E. *Astrophys. J.* **2002**, *574*, L167–L170.
(24) Williams, D. A.; Herbst, E. *Surf. Sci.* **2002**, *500*, 823–837.
(25) Ehrenfreund, P.; Sephton, M. A. *Faraday Discuss.* **2006**, *133*, 277–288.
(26) Pardo, J. R.; Cernicharo, J. *Astrophys. J.* **2007**, *654*, 978–987.
(27) Bohme, D. K. *Chem. Rev.* **1992**, *92*, 1487–1508.
(28) Smith, D. *Chem. Rev.* **1992**, *92*, 1473–1485.
(29) Anicich, V. G. *J. Phys. Chem. Ref. Data* **1993**, *22*, 1469–1569.
(30) Scott, G. B. I.; Fairley, D. A.; Freeman, C. G.; McEwan, M. J.; Adams, N. G.; Babcock, L. M. *J. Phys. Chem. A* **1997**, *101*, 4973–4978.
(31) Anicich, V.; McEwan, M. J. *Planet. Space Sci.* **1997**, *45*, 897–921.
(32) McEwan, M. J.; Scott, G. B. I.; Adams, N. G.; Babcock, L. M.; Terzieva, R.; Herbst, E. *Astrophys. J.* **1999**, *513*, 287–293.
(33) Bernstein, M. P.; Dworkin, J. P.; Sandford, S. A.; Allamandola, L. J. *Meteorit. Planet. Sci.* **2001**, *36*, 351–358.

(34) Dworkin, J.; Deamer, D.; Sandford, S. A.; Allamandola, L. *Proc. Natl. Acad. Sci. U.S.A.* **2001**, *98*, 815−819.
(35) Bernstein, M. P.; Dworkin, J. P.; Sandford, S. A.; Cooper, G. W.; Allamandola, L. J. *Nature* **2002**, *416*, 401−403.
(36) Lebonnois, S. *Planet. Space Sci.* **2005**, *53*, 486−497.
(37) Rhee, Y. M.; Lee, T. J.; Gudipati, M. S.; Allamandola, L. J.; Head-Gordon, M. *Proc. Natl. Acad. Sci. U.S.A.* **2007**, *104*, 5274−5278.
(38) Gudipati, R. S.; Allamandola, L. J. *Astrophys. J.* **2006**, *638*, 286−292.
(39) Le Page, V.; Snow, T. P.; Bierbaum, V. M. *Astrophys. J. Suppl. Ser.* **2001**, *132*, 233−251.
(40) Coates, A. J.; Crary, F. J.; Lewis, G. R.; Young, D. T.; Waite, J. H.; Sittler, E. C. *Geophys. Res. Lett.* **2007**, *34*, L22103−L22109.
(41) Vuitton, V.; Yelle, R. V.; Cui, J. *J. Geophys. Res.* **2008**, *113*, E05007−E05025.
(42) Ricketts, C. L.; Schrçder, D.; Alcaraz, C.; Roithov, J. *Chem.-Eur. J.* **2008**, *14*, 4779−4783.
(43) Coates, A. J. *Philos. Trans. R. Soc., A* **2009**, *367*, 773−788.
(44) Delitsky, M. L.; McKay, C. P. *Icarus* **2010**, *207*, 477−484.
(45) Fegley, B. *Space Sci. Rev.* **1999**, *90*, 239−252.
(46) Alexander, C. M. O'D.; Boss, A. P.; Carlson, A. W. *Science* **2001**, *294*, 64−68.
(47) Herbst, E.; Adams, N. G.; Smith, D.; DeFree, D. J. *Astrophys. J.* **1987**, *312*, 351−357.
(48) Herbst, E. *J. Phys. Chem. A* **2005**, *109*, 4017−4029.
(49) Momoh, P. O.; Soliman, A. R.; Meot-Ner, M.; Ricca, A.; El-Shall, M. S. *J. Am. Chem. Soc.* **2008**, *130*, 12848−12849.
(50) Soliman, A.; Hamid, A. M.; Abrash, S. A.; El-Shall, M. S. *Chem. Phys. Lett.* **2012**, *523*, 25−33.
(51) Ricca, A.; Bauschlicher, C. W., Jr.; Bakes, E. L. O. *Icarus* **2001**, *154*, 516−521.
(52) Ricca, A.; Baushlicher, C. W., Jr.; Rosi, M. *Chem. Phys. Lett.* **2001**, *347*, 473−480.
(53) Bauschlicher, C. W., Jr.; Ricca, R.; Rosi, M. *Chem. Phys. Lett.* **2002**, *347*, 159−163.
(54) Ascenzi, D.; Aysina, J.; Tosi, P.; Maranzana, A.; Tonachini, G. *J. Chem. Phys.* **2010**, *133*, 184308−184317.
(55) El-Shall, M. S.; Ibrahim, Y. M.; Alsharaeh, E. H.; Meot-Ner, M.; Watson, S. P. *J. Am. Chem. Soc.* **2009**, *131*, 10066−10076.
(56) Momoh, P. O.; Abrash, S. A.; Mabourki, R.; El-Shall, M. S. *J. Am. Chem. Soc.* **2006**, *128*, 12408−12409.
(57) Momoh, P. O.; Hamid, A. M.; Abrash, S. A.; El-Shall, M. S. *J. Chem. Phys.* **2011**, *134*, 204315−204328.
(58) Soliman, A.; Hamid, A. M.; Momoh, P. O.; El-Shall, M. S.; Taylor, D.; Gallagher, L.; Abrash, S. A. *J. Phys. Chem. A* **2012**, *116*, 8925−8933.
(59) El-Shall, M. S. *Acc. Chem. Res.* **2008**, *41*, 783−792.
(60) Rusyniak, M.; Ibrahim, Y.; Wright, D.; Khanna, S.; El-Shall, M. S. *J. Am. Chem. Soc.* **2003**, *125*, 12001−12013.
(61) Mason; E. A.; McDaniel, E. W. *Transport Properties of Ions in Gases*; John Wiley & Sons: New York, 1988.
(62) Frisch, M. J.; Trucks, G. W.; Schlegel, H. B.; Scuseria, G. E.; Robb, M. A.; Cheeseman, J. R.; Zakrzewski, V. G.; Montgomery, J. A.; Stratmann, R. E.; Burant, J. C.; Daprich, S.; Millam, J. M.; Daniels, A. D.; Kudin, K. N.; Strain, M. C.; Farkas, O.; Tomasi, J.; Barone, V.; Cossi, M.; Cammi, R.; Mennucci, B.; Pomelli, C.; Adamo, C.; Clifford, S.; Ochterski, J.; Petersson, G. A.; Ayala, P. Y.; Cui, Q.; Morokuma, K.; Malick, D. K.; Rabuck, A. D.; Raghavachari, K.; Foresman, J. B.; Cioslowski, J.; Ortiz, J. V.; Baboul, A. G.; Stefanov, B. B.; Liu, G.; Liashenko, P.; Piskorz, P.; Komaromi, I.; Gomperts, R.; Martin, R. L.; Fox, D. J.; Keith, T.; Al-Laham, M. A.; Peng, C. Y.; Nanayakkara, A.; Gonzalez, C.; Challacombe, M.; Gill, P. M. W.; Johnson, B. G.; Chen, W.; Wong, M. W.; Andres, J. L.; Gonzalez, C.; Head-Gordon, M.; Replogle, E. S.; Pople, J. A. *Gaussian 03*, revision C.02; Gaussian, Inc.: Pittsburgh, PA, 2004.
(63) Mesleh, M. F.; Hunter, J. M.; Shvatsburg, A. A.; Schatz, G. C.; Jarrold, M. F. *J. Phys. Chem.* **1996**, *100*, 16082−16086.
(64) Yao, S.; Zhang, X.; Zhang, L.; Wang, C.; Guo, Y. *Rapid Commun. Mass Spectrom.* **2007**, *21*, 1739−1744.
(65) Meot-Ner, M.; Sieck, L. W.; El-Shall, M. S.; Daly, G. M. *J. Am. Chem. Soc.* **1995**, *117*, 7737−7743.
(66) Ibrahim, Y. M.; Meot-Ner, M.; El-Shall, M. S. *J. Phys. Chem. A* **2006**, *110*, 8585−8592.
(67) El-Shall, M. S.; Marks, C. *J. Phys. Chem.* **1991**, *95*, 4932−4935.
(68) El-Shall, M. S.; Schriver, K. E. *J. Chem. Phys.* **1991**, *95*, 3001−3003.
(69) El-Shall, M. S.; Daly, G. M.; Yu, Z.; Meot-Ner, M. *J. Am. Chem. Soc.* **1995**, *117*, 7744−7752.
(70) El-Shall, M. S.; Yu, Z. *J. Am. Chem. Soc.* **1996**, *118*, 13058−13068.
(71) Pithawalla, Y. B.; Gao, J.; Yu, Z.; El-Shall, M. S. *Macromolecules* **1996**, *29*, 8558−8561.
(72) Mahmoud, H.; Germanenko, I. N.; El-Shall, M. S. *J. Phys. Chem. A* **2006**, *110*, 4296−4298.
(73) von Helden, G.; Kemper, P. R.; Gotts, N. G.; Bowers, M. T. *Science* **1993**, *259*, 1300−1302.
(74) Lee, S.; Gotts, N. G.; Von Helden, G.; Bowers, M. T. *Science* **1995**, *267*, 999−1001.
(75) Shvartsburg, A. A.; Hudgins, R. R.; Dugourd, P.; Jarrold, M. F. *J. Phys. Chem.* **1997**, *101*, 1684−1688.
(76) Alsharaeh, E. H.; Ibrahim, Y. M.; El-Shall, M. S. *J. Am. Chem. Soc.* **2005**, *127*, 6164−6165.